PAPER

Check for updates

Room-temperature spin-conserved electron transport to semiconductor quantum dots using a superlattice barrier†

Satoshi Hiura, ID *[a] Saeko Hatakeyama,[a] Mattias Jansson, ID [b] Junichi Takayama, ID [a] Irina Buyanova, ID [b] Weimin Chen ID [b] and Akihiro Murayama ID [a]

To realize the optical transfer of electron spin information, developing a semiconductor layer for efficient transport of spin-polarized electrons to the active layers is necessary. In this study, electron spin transport from a GaAs/Al$_{0.3}$Ga$_{0.7}$As superlattice (SL) barrier to In$_{0.5}$Ga$_{0.5}$As quantum dots (QDs) is investigated at room temperature through a combination of time-resolved photoluminescence and rate equation analysis, separating the two transport processes from the GaAs layer around the QDs and SL barrier. The electron transport time in the SL increases for a thicker quantum well (QW) of SL due to the weaker wavefunction overlap between adjacent QWs. Additionally, the degree of conservation of spin polarization during transport varies with QW thickness. Rate equation analysis demonstrates an electron transport from SL to QDs while maintaining a high spin polarization for thick QWs. The achieved spin-conserved electron transport can be attributed to the combination of electron transport being sufficiently faster than the spin relaxation in SL and the suppressed spin relaxation in the p-doped GaAs layer capping the QDs. The findings indicate that SL is a promising candidate as an electron spin transport layer for optical spin devices.

1. Introduction

In recent years, opto-spintronics has gained significant interest for integrating spin-based information processing/memory and optical information transfer/communication.[1,2] The fusion of spintronics and photonics is essential for the realization of energy-saving information systems.[3,4] The optical transfer of electron spin information requires using opto-semiconductor materials such as III–V semiconductors. However, the spin polarization of electrons is rapidly lost in non-magnetic III–V semiconductors, hindering the long-term retention of electron spin information. Generally, III–V semiconductor quantum dots (QDs) are promising spin-photon interfaces owing to their long spin lifetime[5–7] and excellent light emission properties.[8–11] Significant efforts have been directed to develop spin-polarized light-emitting diodes (LEDs) using QDs as an active layer,[3,12–18] emitting circularly polarized light reflecting the spin-polarized state of electrons. The performance of spin LEDs is affected by spin relaxation

occurring during electron transport from the ferromagnetic spin injector to the active layer. The degree of spin conservation during transport in a GaAs barrier is less than 30% at room temperature (RT).[17] Large spin depolarization mainly originates from D'yakonov–Perel' spin relaxation, which is dominant at high temperatures.[19–21] Therefore, developing an electron spin transport layer that retains high spin polarization is necessary.

Using a superlattice (SL) as an electron spin-transport layer is a candidate approach for transporting spin-polarized electrons to active layers. Previous studies have demonstrated electron spin transport from a GaAs/AlGaAs SL to InGaAs QDs using quantum waves at low temperatures,[22,23] where the spin polarization of electrons is fully conserved during wavefunction penetration. Such quantum spin transport is expected to suppress electron spin relaxation owing to scattering. Recent studies have investigated the effects of AlGaAs barrier thickness and growth temperature on the spin-relaxation properties of GaAs/AlGaAs SL at RT.[24,25] The spin-relaxation time is faster for a thinner AlGaAs barrier because an enhanced in-plane effective magnetic field promotes spin relaxation. Additionally, the spin relaxation of SL can be affected by quantum well (QW) thickness. In multiple GaAs/AlGaAs QWs, D'yakonov–Perel' interaction is a dominant spin-relaxation mechanism at RT;[26] thus, spin relaxation time depends on electron confinement energy.[20,26–28] Furthermore, the wavefunction overlap between adjacent QWs varies with the QW thickness of SL, capable

[a] *Faculty of Information Science and Technology, Hokkaido University, Sapporo 060-0814, Japan. E-mail: hiura@ist.hokudai.ac.jp*

[b] *Department of Physics, Chemistry and Biology, Linköping University, 58183 Linköping, Sweden*

† Electronic supplementary information (ESI) available. See DOI: https://doi.org/10.1039/d4cp03973d

2210 | *Phys. Chem. Chem. Phys.*, 2025, **27**, 2210–2217
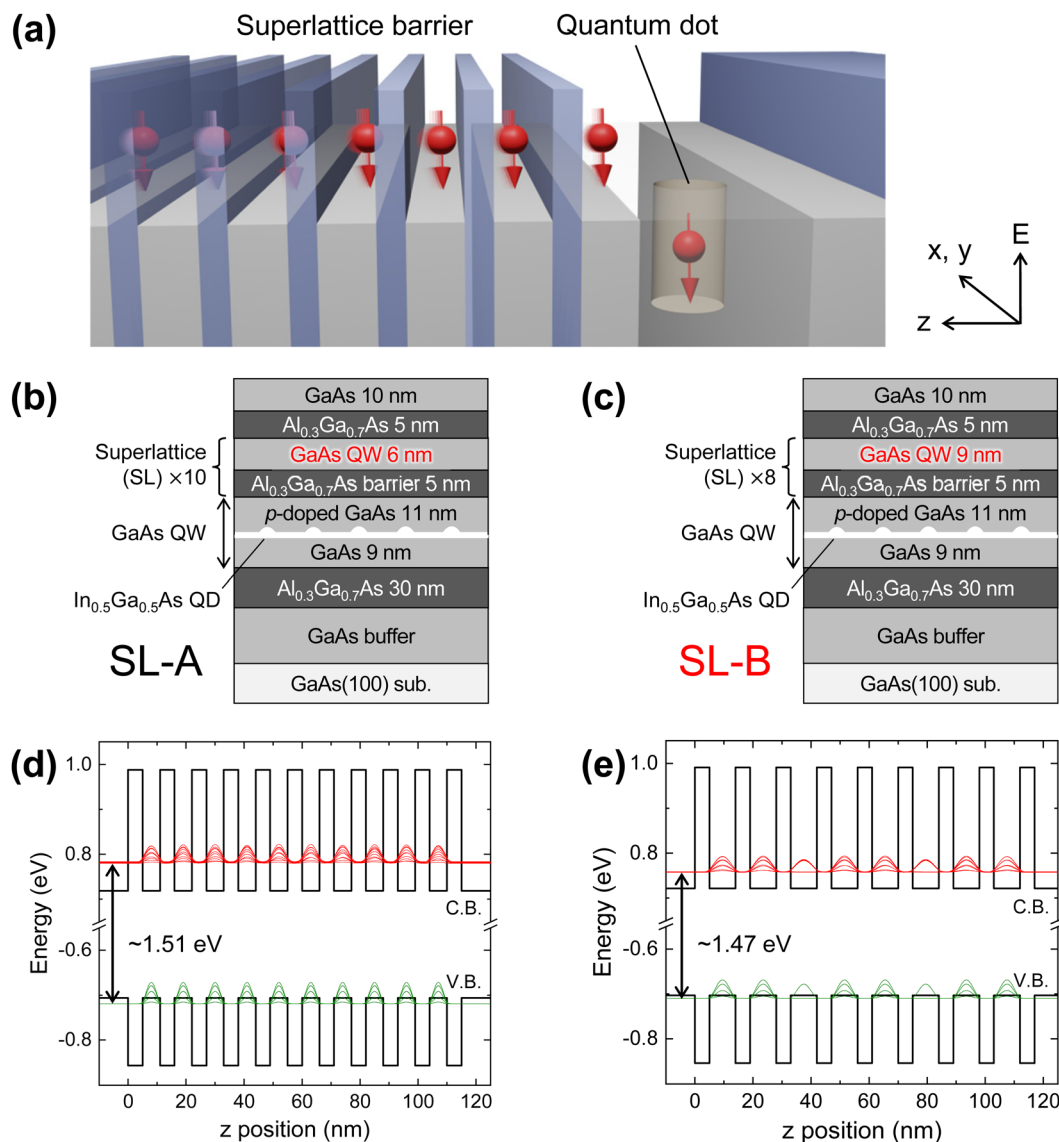
This journal is © the Owner Societies 2025

Fig. 1 (a) Schematic illustration of spin-conserved electron transport from superlattice (SL) barrier to quantum dot (QD). Schematic sample structure of (b) SL-A with QW thickness of 6 nm and (c) SL-B with QW thickness of 9 nm. One-dimensional band calculation of GaAs/Al$_{0.3}$Ga$_{0.7}$As SL with electron and hole wavefunctions in the miniband for (d) SL-A and (e) SL-B.

of changing electron transport time in SL. However, the effects of QW thickness on the electron spin transport properties of SL have not been explored at RT. For applications to QD spin LEDs, understanding the electron spin transport from the SL barrier to QDs is crucial.

This study investigates at RT the electron spin transport from GaAs/AlGaAs SL to InGaAs QDs using time-resolved circularly polarized photoluminescence (PL) in combination with rate equation analysis. The electron transport time decreases for thicker QWs due to the weaker overlap of wave functions between adjacent QWs. The spin polarization of electrons transported from SL to QDs depends on the QW thickness. Rate equation analysis reveals the achievement of spin-conserved electron transport from the SL to QDs. The efficient transport of spin-polarized electrons in SL illustrated in Fig. 1a can be attributed to the combination of electron transport before promoting spin

relaxation and suppression of spin relaxation in the p-doped GaAs layer capping the QDs.

2. Experimental

2.1. Sample preparation

Schematic illustrations of two sample structures prepared by molecular beam epitaxy are shown in Fig. 1b and c. First, a 400-nm-thick GaAs buffer layer was grown on a semi-insulating GaAs(100) substrate. Then, a 30-nm-thick Al$_{0.3}$Ga$_{0.7}$As barrier layer was grown to confine photo-excited electrons and holes in the QD emissive layer. After the subsequent growth of a 9-nm-thick GaAs layer, a single layer of 7.5-ML-thick In$_{0.5}$Ga$_{0.5}$As QDs was grown at 773 K. The QDs were capped with an 11-nm-thick GaAs layer with Be doping (3×10^{17} cm^{-3}) at the same temperature, followed by the growth of SL barriers. Notably,

This journal is © the Owner Societies 2025

Phys. Chem. Chem. Phys., 2025, **27**, 2210–2217 | **2211**

the In$_{0.5}$Ga$_{0.5}$As QDs were embedded in a 20-nm-thick GaAs QW. Such a dot-in-well structure enabled efficient carrier injection into the QDs.[29] The SL barriers comprised 10 repeats of 6-nm-thick GaAs QW and 5-nm-thick Al$_{0.3}$Ga$_{0.7}$As barrier, or 8 repeats of 9-nm-thick GaAs QW and 5-nm-thick Al$_{0.3}$Ga$_{0.7}$As barrier. A 5-nm-thick Al$_{0.3}$Ga$_{0.7}$As layer was grown on the SL barrier and capped with a 10-nm-thick GaAs layer. The growth temperatures of the layers excluding the QDs and their capping layers were set to 853 K. Hereafter, samples with 6-nm-thick QW and 9-nm-thick QW SL layers are labeled SL-A and SL-B, respectively. The two samples exhibit similar SL barrier thicknesses.

Fig. 2 High-angle annular dark-field scanning transmission electron microscopy images of (a) SL-A and (b) SL-B, where the regions from the bottom Al$_{0.3}$Ga$_{0.7}$As layers to the SL layers are visible. The insets show typical high-resolution high-angle annular dark-field scanning transmission electron microscopy images of buried In$_{0.5}$Ga$_{0.5}$As QDs.

2.2. Optical characterization

Circularly polarized PL and time-resolved experiments were conducted at RT using a streak camera combined with a spectrometer under σ^+-polarized excitation. The excitation energies were mainly changed from 1.39 to 1.59 eV, excluding those for PL excitation measurements. The excitation energies were set to 1.51 and 1.47 eV to selectively excite the SL heavy-hole states of SL-A and SL-B, respectively (Fig. 1d, e and 3b). Both the excitation and detection directions coincided with the sample growth direction. A mode-locked Ti:Sapphire pulsed laser with a repetition rate of 80 MHz, pulse width of <100 fs, and spectral width of 10 nm was used as the excitation source. The laser spot diameter was ∼50 μm. The full-width half maximum of the laser pulse time response curve was ∼11 ps. To characterize polarization-resolved optical properties, a linear polarizer and a quarter-wave plate were inserted into the excitation (detection) beam paths to generate (detect) circularly polarized excitation (emission). For this study, the spin polarization of electrons generated in the GaAs layers was expected to be 50% according to the optical selection rule when considering valence-band mixing. The circular polarization degree (CPD) of QD PL is defined as $(I_{\sigma^+} - I_{\sigma^-})/(I_{\sigma^+} + I_{\sigma^-})$ using the circularly polarized PL intensity $I_{\sigma^\pm}$, reflecting the spin polarization of electrons at QD emissive states. For PL excitation measurements at RT, a tunable Ti:Sapphire laser was used as the excitation source. In this study, the GaAs capping layer was p-doped to supply holes to the QDs. Furthermore, p-doping can lead to a hole-rich condition in the QDs. Therefore, PL and the CPD properties of QDs were expected to depend on the electron spins injected into the QDs. One-dimensional band structures of the SL and wavefunctions of electrons and holes were calculated using the nextnano software.[30]

3. Results and discussion

The high-angle annular dark-field scanning transmission electron microscopy images of the In$_{0.5}$Ga$_{0.5}$As QDs and GaAs/Al$_{0.3}$Ga$_{0.7}$As SL structures for SL-A and SL-B are shown in Fig. 2a and b, respectively. The results indicated the formation of atomically flat GaAs/Al$_{0.3}$Ga$_{0.7}$As interfaces. Sharp interfaces significantly reduced the interfacial roughness scattering of tunneling electrons, which suppressed spin relaxation by
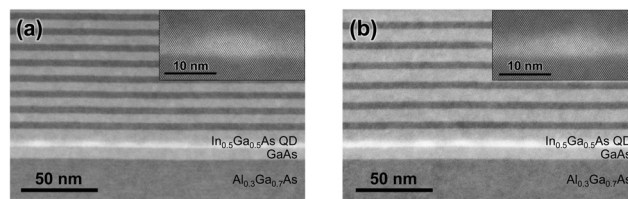
tunneling between adjacent GaAs QWs. Notably, electron tunneling time was expected to differ between the two samples. As the QW of SL-A was thinner than that of SL-B, the electron miniband energy was higher for SL-A (Fig. 1d and e). Consequently, the overlap of electron wavefunctions between adjacent QWs was stronger for SL-A, implying faster electron tunneling. Contrarily, weaker wavefunction overlap for SL-B facilitates radiative recombination of electrons and holes within QWs during PL measurements and reduces the efficiency of electron transport from SL to QDs. Buried In$_{0.5}$Ga$_{0.5}$As QDs are shown in Fig. 2a and b. As shown in the insets, the typical QD diameters/heights of SL-A and SL-B were estimated as 21/3.5 and 25/4.2 nm, respectively. The formation of differently sized QDs was attributed to time-varying growth conditions, such as growth rate and arsenic pressure.

An overview of the PL spectra of the two samples measured at excitation energies above the SL miniband states is shown in Fig. 3a. Four PL peaks were observed for both samples. PL peak energies of 1.23 and 1.20 eV for SL-A and SL-B originated from the QD ground states, respectively. The lower energy shift of SL-B was attributed to a large QD size, confirmed by scanning transmission electron microscopy observations. For QD PL from the first excited state, the PL peak energy was 1.26 eV for SL-B as compared to 1.29 eV for SL-A. Small PL peaks at 1.43 eV for both samples originated from the 20-nm-thick GaAs QWs surrounding the QDs. PL peak energies of 1.51 and 1.47 eV for SL-A and SL-B originated from SL miniband states, respectively. The PL excitation spectra detected in the QD ground states are shown in Fig. 3b, where distinct features related to the heavy-hole and light-hole states are observed. The heavy hole energies of SL-A and SL-B were located at 1.51 and 1.47 eV, respectively. The values were consistent with the band-calculation results shown in Fig. 1d and e. The obtained PL/PL excitation results provided experimental evidence of SL structures designed with sharp GaAs/Al$_{0.3}$Ga$_{0.7}$As interfaces. Furthermore, different intensity ratios of QD PL to SL PL of the two samples are shown in Fig. 3a. A stronger SL PL of SL-B compared to that of SL-A was related to a smaller wavefunction penetration into adjacent QWs. For SL-B, the dominant radiative recombination within SL reduced the electron transport efficiency, resulting in a lower QD PL intensity. The QD PL spectra at the excitation of a 20-nm-thick GaAs QW and SL miniband are shown in Fig. 3c. The PL intensities were normalized to the peak PL intensity at the GaAs QW excitation. For both samples, the QD PL intensity

2212 | *Phys. Chem. Chem. Phys.*, 2025, **27**, 2210–2217

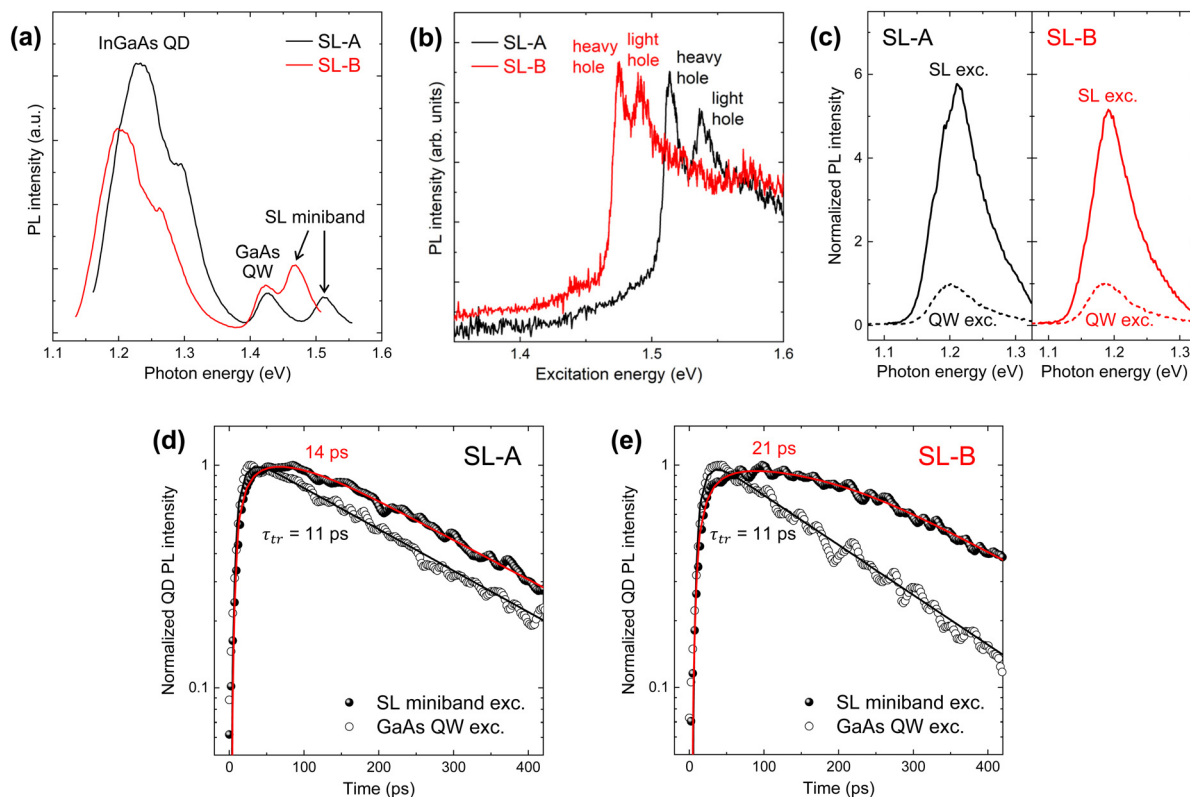This journal is © the Owner Societies 2025

Fig. 3   (a) Overview of PL spectra at an excitation energy above SL miniband. (b) PL excitation spectra detected at QD ground state. (c) QD PL spectra at excitations of GaAs QW and SL, where the PL intensities are normalized to the peak PL intensity at an excitation of GaAs QW. Normalized PL time profiles of QD excited states at excitations of GaAs QW and SL for (d) SL-A and (e) SL-B. The solid lines indicate the best-fitted rate equation results.

increased significantly upon excitation of the SL miniband relative to the excitation of the GaAs QW. The increase was slightly greater for SL-A. Considering that the total thickness of the SL-QW layers to be excited was greater for SL-B, the obtained result supported a lower electron transport efficiency.

The difference in electron transport properties between the two samples was observed from the time-dependent PL behavior. The normalized PL time profiles of the QD excited states for SL-A and SL-B are shown in Fig. 3d and e, respectively, measured at the excitations of the GaAs QWs and SL minibands. At SL miniband excitation, a slower PL increase was observed for SL-B than for SL-A. To examine the electron transport time (τ_{tr}), rate equation analysis of the PL time profiles was performed (details are provided in Supplementary note S1, ESI†). The same value of τ_{tr} = 11 ps was obtained at an excitation of GaAs QW, whereas τ_{tr} = 21 ps for SL-B was longer than τ_{tr} = 14 ps for SL-A at SL miniband excitation. The longer τ_{tr} for SL-B was related to slower electron tunneling between adjacent QWs of the SL, as aforementioned. Conversely, the significant increase in τ_{tr} from 11 to 21 ps indicated the contribution of electrons generated in the SL far from the QDs to the QD light emission. For SL-A, τ_{tr} at SL excitation was close to that at GaAs QW excitation. Thus, fast electron tunneling was observed between the adjacent QWs of SL. Here, note that no significant difference in the electron transport efficiency between the two samples could occur from the perspective of

electrical carrier injection. In PL measurements, holes were generated in the GaAs QW of SL; thus, electrons radiatively recombined with holes during transport. The radiative recombination reduced electron transport efficiency, particularly for SL-B. However, for a p–i–n LED using SL as an electron transport layer, electrons and holes were transported from the opposite direction to the active layer. Thus, radiative recombination within the SL was almost negligible and cannot affect the electron transport efficiency.

Further, the electron spin transport from the SL to the QDs was analyzed. The circularly polarized PL time profiles and the corresponding CPD of the QD excited states for SL-A and SL-B are shown in Fig. 4a and b, respectively, measured upon excitation of the SL miniband. The CPD values during the initial time are shown in the insets. The initial CPD properties of the QD excited states reflected the degree of spin relaxation during transport to QDs.[22,31] Although the heavy-hole and light-hole states were split, as shown in Fig. 3b, the initial spin polarization of electrons generated in the SL was estimated as 50% when considering the valence-band mixing and spectral width of the excitation pulsed laser.[22,23] The initial CPD value of SL-B was higher than that of SL-A. The initial CPD values as a function of the excitation energy are plotted in Fig. 4c. For this study, initial CPD is defined as the mean value near a CPD peak in the initial time region. At GaAs QW excitation, identical values of 26–27% were obtained for the two samples. The values

This journal is © the Owner Societies 2025

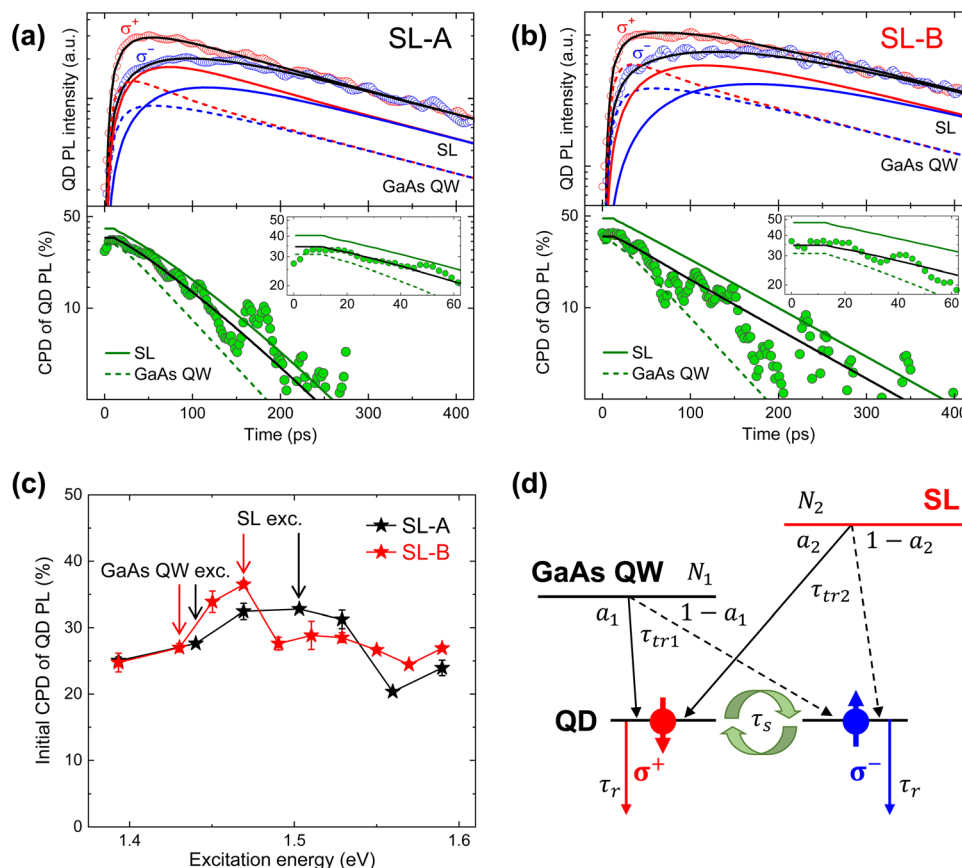*Phys. Chem. Chem. Phys.*, 2025, **27**, 2210–2217 | **2213**

Fig. 4 Circularly polarized PL time profiles and corresponding CPD of QD excited states for (a) SL-A and (b) SL-B, at SL miniband excitation. The insets show the CPD time profiles in the initial time region. The black solid lines indicate the best-fitted rate equation results, which are decomposed into two components, spin-polarized carriers generated in GaAs QW and SL. (c) Initial PL CPD of QD excited states as a function of excitation energy. (d) Schematic model of spin-split rate equation, where the electron spin transport to the QD from the GaAs QW and the SL is considered.

were close to the previously reported values for electron spin injection from the GaAs barrier into InGaAs QDs.[29,32,33] Furthermore, the initial CPD value was dependent on the excitation energy. The value increased to 32% under SL excitation for SL-A, while a significant increase to 37% for SL-B was observed. The results indicated the efficient transport of spin-polarized electrons from SL to QDs while maintaining a high spin polarization for SL-B. Notably, the time-dependent QD PL at SL excitation included electron spin transport from both the GaAs QW around the QDs and the SL. Each component needs to be separated to extract the net spin polarization of the electrons transported from SL to QDs.

To separate the electron spin transport from the GaAs QW and SL, rate equation analysis was performed considering two spin transport processes, as schematically illustrated in Fig. 4d. This rate equation model was employed to extract the net spin polarization of the electrons transported from SL to QDs, because the raw time-dependent circularly polarized PL data of the QDs screen the spin polarization properties of transported electrons. The initial number of excitons generated in the GaAs QW (SL) with σ^+-polarization was expressed by $N_{1(2)}$.

The rate equation was expressed as:

$$\frac{\mathrm{d}N_{\mathrm{QW}}}{\mathrm{d}t} = -\alpha_1 \frac{N_{\mathrm{QW}}}{\tau_{\mathrm{tr1}}} - (1-\alpha_1)\frac{N_{\mathrm{QW}}}{\tau_{\mathrm{tr1}}}, \tag{1}$$

$$\frac{\mathrm{d}N_{\mathrm{SL}}}{\mathrm{d}t} = -\alpha_2 \frac{N_{\mathrm{SL}}}{\tau_{\mathrm{tr2}}} - (1-\alpha_2)\frac{N_{\mathrm{SL}}}{\tau_{\mathrm{tr2}}}, \tag{2}$$

$$\frac{\mathrm{d}N_{\mathrm{QD}}^{\sigma^+}}{\mathrm{d}t} = \alpha_1 \frac{N_{\mathrm{QW}}}{\tau_{\mathrm{tr1}}} + \alpha_2 \frac{N_{\mathrm{SL}}}{\tau_{\mathrm{tr2}}} - \frac{N_{\mathrm{QD}}^{\sigma^+}}{\tau_{\mathrm{r}}} - \frac{N_{\mathrm{QD}}^{\sigma^+}}{\tau_{\mathrm{s}}} + \frac{N_{\mathrm{QD}}^{\sigma^-}}{\tau_{\mathrm{s}}}, \tag{3}$$

$$\frac{\mathrm{d}N_{\mathrm{QD}}^{\sigma^-}}{\mathrm{d}t} = (1-\alpha_1)\frac{N_{\mathrm{QW}}}{\tau_{\mathrm{tr1}}} + (1-\alpha_2)\frac{N_{\mathrm{SL}}}{\tau_{\mathrm{tr2}}} - \frac{N_{\mathrm{QD}}^{\sigma^-}}{\tau_{\mathrm{r}}} - \frac{N_{\mathrm{QD}}^{\sigma^-}}{\tau_{\mathrm{s}}} + \frac{N_{\mathrm{QD}}^{\sigma^+}}{\tau_{\mathrm{s}}}, \tag{4}$$

where the excitons generated in the GaAs QW and SL were transported to the QDs with time constants of τ_{tr1} and τ_{tr2}, respectively. As this study prioritized spin polarization evaluation of electrons transported from SL to QDs, a spin conservation factor during transport was introduced. Parameters α_1 and α_2 were defined as the spin conservation factor during electron transport from the GaAs QW and SL, respectively. Conversely, α_1 and α_2 were dependent on the degree of spin relaxation in the GaAs QW and SL, respectively. Herein, $\alpha_{1,2}$ indicated the

fraction of spin conservation, where a value of 0.5 (0.75) indicated that the spin polarization of transported electrons was 0% (50%). In the model, the parallel-spin electrons $\alpha_1 N_1$ ($\alpha_2 N_2$) were transported from the GaAs QW (SL) to the parallel-spin state of the QDs, whereas the anti-parallel-spin electrons $(1 - \alpha_1)N_1$ $[(1 - \alpha_2)N_2]$ were transported to the opposite spin state. The spin-polarized electrons transported to the QDs relaxed with time constants of spin relaxation (τ_s) and relaxation (τ_r), which included the radiative and non-radiative decay processes. The rate-equation fit results of the PL and CPD time profiles are shown in Fig. 4a and b, combined with a convolution calculation of the time-response curve for the laser pulse. The time profiles were decomposed into two components: electron spin transport from GaAs QW and SL. The fitting parameters are presented in Table 1. For both samples, $\tau_{tr1} = 11$ ps and $\alpha_1 = 0.67$ were fixed based on the rate equation analysis of the circularly polarized PL time profiles at GaAs QW excitation. Herein, τ_{tr2} was longer for SL-B than for SL-A, which supported the slower electron transport. Notably, $\alpha_2 = 0.76$ was obtained for SL-B as compared to $\alpha_2 = 0.72$ for SL-A. The rate-

equation analysis implied that the spin polarization of electrons transported from SL to QDs was approximately 50% for SL-B, indicating spin-conserved electron transport. The results were reflected in the decomposed CPD time profile shown in Fig. 4b (marked as SL), which indicated an initial spin polarization of 48%. As shown in Fig. 4a, a lower initial spin polarization of 40% was obtained for SL-A.

To reveal the origin of the difference in electron spin transport between SL-A and SL-B, the spin relaxation of the SL was investigated. The time-dependent PL CPD of the SL miniband with the single-exponential decay fittings is shown in Fig. 5a. Excitation energies of 1.71 and 1.60 eV were used for SL-A and SL-B, respectively, to excite the second miniband. The initial CPD of SL PL was approximately 27%, whereas the CPD decay properties differed significantly between the two samples. A much longer spin relaxation time $\tau_s = 195$ ps was obtained for SL-B as compared to $\tau_s = 71$ ps for SL-A. The difference in τ_s was interpreted based on the electron confinement energy (E_{1e}). The spin relaxation time obtained as a function of E_{1e} is plotted in Fig. 5b. The least squares fit resulted in $\tau_s \propto E_{1e}^{-20}$, which agreed with the dependence of the spin relaxation time on the electron confinement energy expected in D'yakonov–Perel' theory of QW.[20,34] Therefore, the spin relaxation time of SL was dependent on the D'yakonov–Perel' interaction, and the smaller electron confinement energy in the QW led to a longer spin relaxation time. Thus, the spin-

Table 1 Fitting parameter values of rate equation for SL-A and SL-B

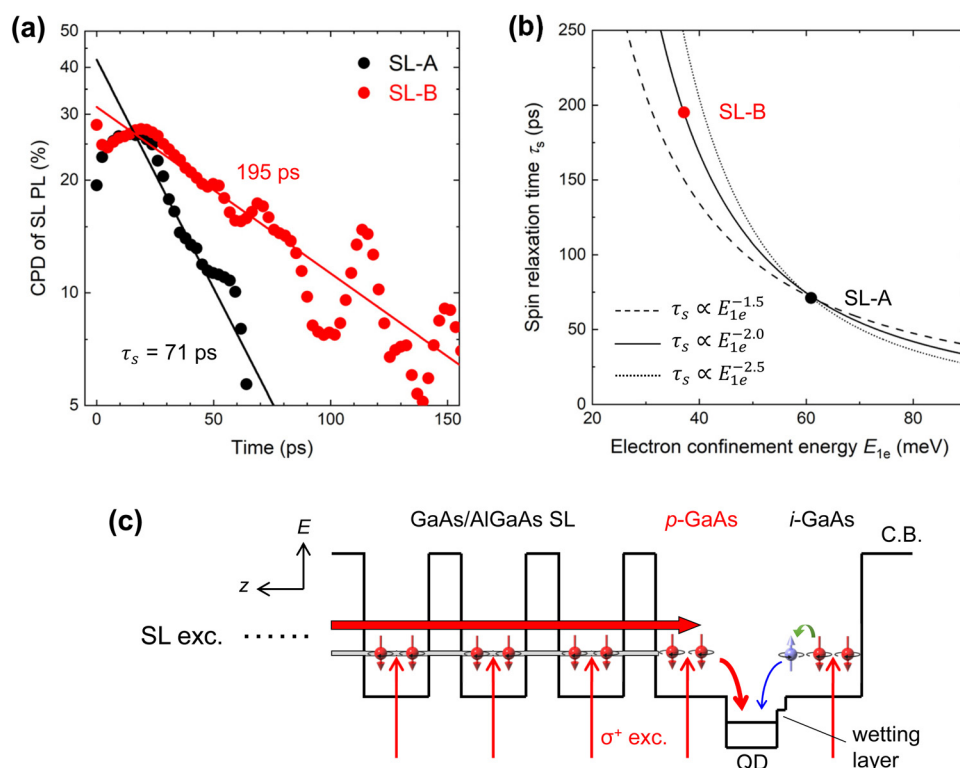|	τ_{tr1} (ps)	α_1	τ_{tr2} (ps)	α_2	τ_r (ps)	τ_s (ps)	N_2/N_1
SL-A	11	0.67	41	0.72	248	120	1.61
SL-B	11	0.67	80	0.76	258	120	1.49

Fig. 5 (a) Time-dependent CPD of SL PL with single-exponential decay fittings (solid lines) for SL-A and SL-B. (b) Spin relaxation time (τ_s) as a function of electron confinement energy (E_{1e}) for SL-A and SL-B. The solid line showing $\tau_s \propto E_{1e}^{-2.0}$ is fitted using the least square method. The dashed and dotted lines showing $\tau_s \propto E_{1e}^{-1.5}$ and $\tau_s \propto E_{1e}^{-2.5}$ through the data point of SL-A are also shown to justify the fitting result, $\tau_s \propto E_{1e}^{-2.0}$. (c) Schematic illustration of electron spin transport dynamics in GaAs QW and SL under the σ^+-polarized excitation of SL miniband.

This journal is © the Owner Societies 2025

Phys. Chem. Chem. Phys., 2025, **27**, 2210–2217 | **2215**

relaxation time of SL at RT could be controlled by changing the QW thickness.

Finally, the electron spin transport dynamics of SL-B with the σ^+-polarized excitation of SL were explored. Under the excitation conditions, the GaAs layers around QDs and SL were excited together, as depicted in Fig. 5c. The spin polarization of electrons injected from the *i*-GaAs barrier into the QDs *via* the wetting layer was expected to be low owing to the rapid spin relaxation in GaAs at RT.[35] The results reflected an initial CPD of 26–27% at GaAs QW excitation (Fig. 4c). Contrarily, the spin polarization of electrons transported from the SL to the QDs *via* p-GaAs capping layer cannot be degraded for the following two reasons. First, spin-polarized electrons can be transported from the SL to the QDs before promoting spin relaxation. The deduced electron transport time, $\tau_{tr2} = 80$ ps, was faster than the spin relaxation time of the SL, $\tau_s = 195$ ps. The net electron transport time should be faster because τ_{tr2} includes the transport time from p-GaAs to QDs. It is also possible that the obtained τ_{tr2} is over-estimated. In these PL measurements, electrons and holes were generated in the SL. In general, hole transport is slower than electron transport because of its higher effective mass. As a result, the QD PL rise time, which is closely related to τ_{tr2}, could be determined by the slower hole transport. In this case, the net electron transport time should be much shorter than the spin-relaxation time. We expect the second advantage to be the use of p-doped GaAs capping layer. A previous study of p-doped InGaAs QDs demonstrated that D'yakonov–Perel' spin relaxation in the p-doped GaAs capping layer can be suppressed at RT through electron-impurity scattering.[17,36] Therefore, we conclude that the combination of electron transport before the promotion of spin relaxation in the SL and suppressed spin relaxation in the p-doped GaAs capping layer results in spin-conserved electron transport from the SL to the QDs even at RT. Future investigations of electron spin transport properties under the application of an electric field will provide valuable insights into the applicability of SL to electron spin transport layers of spin-polarized LEDs and lasers.

4. Conclusions

In summary, the electron spin transport from a GaAs/Al$_{0.3}$Ga$_{0.7}$As SL barrier to In$_{0.5}$Ga$_{0.5}$As QDs was studied at RT through a combination of time-resolved circularly polarized PL and rate equation analysis, separating the two transport processes from the GaAs QW around the QDs and from the SL. The electron transport time in the SL depends on the QW thickness. As the QW thickness increases, the electron transport time increases because of the weaker wavefunction overlap between adjacent QWs. We also found that the degree of spin-polarization conservation during transport depended on the QW thickness. Rate equation analysis demonstrated that electrons could be transported from the SL to the QDs while maintaining a high spin polarization even at RT. The achieved spin-conserved electron transport can be attributed to the combination of electron transport, which is sufficiently faster than spin relaxation in the SL, and the suppression of spin relaxation in the p-doped GaAs layer capping the QDs.

Data availability

The data that support the findings of this study are available from the corresponding authors upon reasonable request.

Author contributions

S. Hiura and A. M. conceived the idea and designed the experiments. S. Hatakeyama prepared the samples by MBE. S. Hiura and S. Hatakeyama performed circularly polarized PL and time-resolved experiments and analyzed the data with the assistance of J. T. PL excitation experiments and data analysis were conducted by M. J. under the supervision of I. B. and W. C. J. T. performed scanning transmission electron microscopy experiments and analyzed the data. S. H. wrote the manuscript. All the authors reviewed and provided feedback on the manuscript.

Conflicts of interest

There are no conflicts to declare.

Acknowledgements

References

1 Y. Huang, V. Polojärvi, S. Hiura, P. Höjer, A. Aho, R. Isoaho, T. Hakkarainen, M. Guina, S. Sato, J. Takayama, A. Murayama, I. A. Buyanova and W. M. Chen, *Nat. Photonics*, 2021, **15**, 475–482.

2 R. Farshchi, M. Ramsteiner, J. Herfort, A. Tahraoui and H. T. Grahn, *Appl. Phys. Lett.*, 2011, **98**, 162508.

3 P. A. Dainone, N. Figueiredo Prestes, P. Renucci, A. Bouché, M. Morassi, X. Deveaux, M. Lindemann, J.-M. George, H. Jaffrès and A. Lemaître, *et al.*, *Nature*, 2024, **627**, 783.

4 S. Hiura, *Nature*, 2024, **627**, 737.

5 A. V. Khaetskii and Y. V. Nazarov, *Phys. Rev. B: Condens. Matter Mater. Phys.*, 2000, **61**, 12639–12642.

6 J. M. Elzerman, R. Hanson, L. H. Willems van Beveren, B. Witkamp, L. M. K. Vandersypen and L. P. Kouwenhoven, *Nature*, 2004, **430**, 431–435.

7 M. Kroutvar, Y. Ducommun, D. Heiss, M. Bichler, D. Schuh, G. Abstreiter and J. J. Finley, *Nature*, 2004, **432**, 81–84.

2216 | *Phys. Chem. Chem. Phys.*, 2025, **27**, 2210–2217

This journal is © the Owner Societies 2025

8 M. Sugawara and M. Usami, *Nat. Photonics*, 2009, **3**, 30–31.

9 S. Chen, W. Li, J. Wu, Q. Jiang, M. Tang, S. Shutts, S. N. Elliott, A. Sobiesierski, A. J. Seeds and I. Ross, *et al.*, *Nat. Photonics*, 2016, **10**, 307.

10 A. Jaffal, W. Redjem, P. Regreny, H. S. Nguyen, S. Cueff, X. Letartre, G. Patriarche, E. Rousseau, G. Cassabois, M. Gendry and N. Chauvin, *Nanoscale*, 2019, **11**, 21847–21855.

11 E. T. Hughes, C. Shang, J. Selvidge, D. Jung, Y. Wan, R. W. Herrick, J. E. Bowers and K. Mukherjee, *Nanoscale*, 2024, **16**, 2966–2973.

12 S. Chakrabarti, M. A. Holub, P. Bhattacharya, T. D. Mishima, M. B. Santos, M. B. Johnson and D. A. Blom, *Nano Lett.*, 2005, **5**, 209–212.

13 C. H. Li, G. Kioseoglou, O. M. J. van't Erve, M. E. Ware, D. Gammon, R. M. Stroud, B. T. Jonker, R. Mallory, M. Yasar and A. Petrou, *Appl. Phys. Lett.*, 2005, **86**, 132503.

14 L. Lombez, P. Renucci, P. F. Braun, H. Carrère, X. Marie, T. Amand, B. Urbaszek, J. L. Gauffier, P. Gallo and T. Camps, *et al.*, *Appl. Phys. Lett.*, 2007, **90**, 2005–2008.

15 F. Cadiz, A. Djeffal, D. Lagarde, A. Balocchi, B. Tao, B. Xu, S. Liang, M. Stoffel, X. Devaux and H. Jaffres, *et al.*, *Nano Lett.*, 2018, **18**, 2381–2386.

16 A. E. Giba, X. Gao, M. Stoffel, X. Devaux, B. Xu, X. Marie, P. Renucci, H. Jaffrès, J.-M. George and G. Cong, *et al.*, *Phys. Rev. Appl.*, 2020, **14**, 034017.

17 K. Etou, S. Hiura, S. Park, K. Sakamoto, J. Takayama, A. Subagyo, K. Sueoka and A. Murayama, *Phys. Rev. Appl.*, 2021, **16**, 014034.

18 K. Etou, S. Hiura, S. Park, J. Takayama, A. Subagyo, K. Sueoka and A. Murayama, *Phys. Rev. Appl.*, 2023, **19**, 024055.

19 M. I. D'yakonov and V. I. Perel, *Zh. Eksp. Teor. Fiz.*, 1973, **65**, 362. Optical orientation in a system of electrons and lattice nuclei in semiconductors. *Theory Sov. Phys. JETP*, 1974, 38, 177.

20 R. S. Britton, T. Grevatt, A. Malinowski, R. T. Harley, P. Perozzo, A. R. Cameron and A. Miller, *Appl. Phys. Lett.*, 1998, **73**, 2140–2142.

21 M. I. Miah, *J. Phys. D: Appl. Phys.*, 2008, **41**, 035105.

22 S. Hiura, K. Itabashi, K. Takeishi, J. Takayama, T. Kiba and A. Murayama, *Appl. Phys. Lett.*, 2019, **114**, 072406.

23 S. Hiura, S. Hatakeyama, J. Takayama and A. Murayama, *Appl. Phys. Lett.*, 2020, **116**, 262407.

24 Y. Ohno, S. Iba, R. Okamoto, Y. Obata, K. Obu, J. J. P. Domingez and H. Saito, *Appl. Phys. Express*, 2020, **13**, 123003.

25 S. Iba, R. Okamoto, K. Obu, Y. Obata and Y. Ohno, *Micromachines*, 2021, **12**, 1112.

26 A. Tackeuchi, Y. Nishikawa and O. Wada, *Appl. Phys. Lett.*, 1996, **68**, 797–799.

27 A. Tackeuchi, T. Kuroda, S. Nishikawa and O. Wada, *Jpn. J. Appl. Phys.*, 1999, **38**, 4680.

28 A. Malinowski, R. S. Britton, T. Grevatt, R. T. Harley, D. A. Ritchie and M. Y. Simmons, *Phys. Rev. B: Condens. Matter Mater. Phys.*, 2000, **62**, 13034–13039.

29 S. Hiura, M. Takishita, J. Takayama, S. Sato and A. Murayama, *Phys. Rev. Appl.*, 2020, **14**, 044011.

30 S. Birner, T. Zibold, T. Andlauer, T. Kubis, M. Sabathil, A. Trellakis and P. Vogl, *IEEE Trans. Electron Devices*, 2007, **54**, 2137–2142.

31 H. Kise, S. Hiura, S. Park, J. Takayama, K. Sueoka and A. Murayama, *Appl. Phys. Lett.*, 2023, **122**, 232405.

32 S. Park, S. Hiura, J. Takayama, K. Sueoka and A. Murayama, *Adv. Electron. Mater.*, 2022, **8**, 2200588.

33 S. Park, S. Hiura, H. Kise, J. Takayama, K. Sueoka and A. Murayama, *Nanoscale*, 2023, **15**, 16784–16794.

34 M. I. D'yakonov and V. Y. Kachorovski, *Sov. Phys. Semicond.*, 1986, **20**, 110.

35 S. Oertel, J. Hübner and M. Oestreich, *Appl. Phys. Lett.*, 2008, **93**, 132112.

36 S. Sato, S. Hiura, J. Takayama and A. Murayama, *Appl. Phys. Lett.*, 2008, **116**, 182401.

This journal is © the Owner Societies 2025

Phys. Chem. Chem. Phys., 2025, **27**, 2210–2217 | **2217**